Current Research in Microbial Sciences 8 (2025) 100345

Contents lists available at ScienceDirect

Current Research in Microbial Sciences

journal homepage: www.sciencedirect.com/journal/current-research-in-microbial-sciences

A novel mode of histone-like protein HupB regulating *Sinorhizobium meliloti* cell division through lysine acetylation

Ningning Li [a,1], Huibo Jin [a,1], Hongbo Li [a], Huilin Yu [a], Xiaoxu Wu [a], Tianci Zhang [a], Liangliang Yu [a], Zhaoling Qin [b], Li Luo [a,*]

[a] *Shanghai Key Laboratory of Bio-energy Crops, Center of Plant Science, School of Life Sciences, Shanghai University, Shanghai 200444, China*
[b] *Department of Microbiology, Naval Medical University, Shanghai 200433, China*

ARTICLE INFO

Keywords:
HU
Acetylation
Lysine
Cell division
Transcriptional regulation

ABSTRACT

HU, a small, basic histone-like protein, binds to bacterial genomic DNA, influencing DNA conformation, replication, and transcription. Its acetylation is a key post-translational modification affecting its DNA-binding activity. The role of HU acetylation in regulating cell division through the cell cycle regulatory system remained largely unknown. In this study, we find that stimulation of lysine acetylation or non-acetylation in HupB, a homolog of HU, differentially regulates the expression of cell cycle regulators, as well as cell growth and division in *Sinorhizobium meliloti*. Lys3, Lys13, and Lys83 in HupB were identified as acetylated residues by mass spectrometry. Mutating these residues to arginine (stimulating non-acetylation) in HupB impedes normal cell division, while substituting them with glycine (mimicking acetylation) allows for rapid cell duplication. The mimicry of non-acetylated HupB leads to enlarged abnormal cells, while stimulating acetylated HupB only reduces cell length. Transcription activation was observed in the mutant cells. Cell cycle regulators such as CtrA, GcrA and DnaA were differentially expressed in the mutants. HupB substitutions differentially bound to these cell cycle regulatory genes. These findings suggest that the appropriate acetylation of HupB regulates the expression of cell cycle regulators, thereby controlling *S. meliloti* cell division.

1. Introduction

The HU protein in *Escherichia coli* is a member of the nuclear-associated protein DNABII family. Comprising two subunits, α and β, it forms heterodimers *in vivo* (Kano et al., 1985). This protein is capable of binding and compressing single-stranded DNA, double-stranded DNA with special structures, as well as RNA (Balandina et al., 2002). Notably, it is involved in the formation of negative DNA supercoils and DNA compaction (Hammel et al., 2016). The HU protein plays a regulatory role in various DNA-related functions, including replication initiation, inversion, phage Mu transposition, DNA repair, and gene expression, akin to eukaryotic histones (Balandina et al., 2001; Holowka et al., 2017; Kamashev and Rouviere-Yaniv, 2000). The deletion of both subunits affects the transcription of approximately 1500 genes, encompassing translation and stress response genes, which underscores the HU protein' significance in transcriptional regulation in *E. coli* (Prieto et al., 2012; Stojkova et al., 2019). Interestingly, the HU deletion mutant in *E. coli* exhibits multiple phenotypes, suggesting that the transcriptional changes in the mutant might not be directly caused by the HU protein itself but rather by the affected transcription factors (Remesh et al., 2020). Consequently, the exact role of the HU protein in gene expression remains largely elusive.

The use of pan-acetyl-lysine antibody immunoprecipitation coupled with high-resolution mass spectrometry techniques has uncovered that HU proteins have extensive acetylation at lysine residues across various bacterial species (Carabetta, 2021). K3, K18, and K86 are the most conserved acetylation sites among these bacteria. These conserved, positively charged lysine residues of HU proteins directly engage with the DNA backbone. The acetylation sites of HU proteins are distributed across three regions (Swinger and Rice, 2004). The first region is located within the initial 20 amino acids of the N-terminus, where nearly every bacterium exhibits at least one acetylation site. The second region is found in the middle of the protein, spanning approximately 40 amino acids, with lower conservation of modification sites. The third region is

* Corresponding author.
E-mail address: liluo@shu.edu.cn (L. Luo).
[1] These authors equally contribute to this paper.

https://doi.org/10.1016/j.crmicr.2025.100345

Available online 22 January 2025

situated at the C-terminus, comprising 25 amino acids, and features multiple modification sites. Acetylation within the DNA binding domain of the HU protein partially neutralizes the positive charge of the lysine side chains, thereby affecting their DNA binding activity.

The acetylation of HU homologous proteins and its effects on physiological functions have been a subject of intense research in recent years. For instance, in *Acinetobacter baumannii*, the 13th lysine of the HU protein is acetylated (Liao et al., 2017). Unlike *E. coli*, the HU in *A. baumannii*, encoded by *hupB*, forms a homodimer. This acetylation does not change the proteins' polymer state but reduces its thermal stability. The acetylated HU protein at K13 shows significantly different DNA binding and dissociation constants compared to the non-acetylated form, suggesting that it acts as an epigenetic regulatory factor controlling HU activity (Liao et al., 2017).

HBsu, similar to HU, binds non-specifically to curved DNA and aids in its compression in the nucleoid of the Gram-positive bacterium *Bacillus subtilis* (Köhler and Marahiel, 1998). Encoded by a single gene, HBsu also forms a homodimer and is essential for the growth of *B. subtilis* (Micka and Marahiel, 1992). It plays a role in DNA recombination and repair. Proteomic analyses have revealed acetylated lysine residues on HBsu, with seven of these residues being studied for their role in nucleoid compression (Kohler and Marahiel, 1997). Mutating lysine to arginine mimics the non-acetylation and enhances nucleoid compression, while mutating to glutamine simulates acetylation, leading to reduced DNA content. This indicates that acetylation of HBsu regulates DNA replication activity (Karaboja and Wang, 2022). One mutant, $HBsu^{K41Q}$, shows a significant reduction in affinity for both HBsu and DNA (Köhler and Marahiel, 1998). Therefore, it is probable that acetylation of HU homologs modulates bacterial cell division or cell cycle progression.

In recent years, advancements in bacterial molecular cell biology have led to the discovery of a cell cycle control mechanism in *Caulobacter crescentus*, a model α-proteobacterium. This mechanism revolves around the response regulator protein CtrA, along with DnaA and GcrA (van Teeseling and Thanbichler, 2020). It modulates cell division by detecting changes in temporal and spatial signals through histidine kinases like CckA, DivL, DivJ, and PhdS. These kinases autophosphorylate and then pass the phosphate groups to downstream phospho-transfer proteins, such as DivK and ChpT. Ultimately, these phosphate groups are transferred to CtrA, which directly controls the expression of over 300 genes, influencing processes like DNA replication, cell division, and differentiation (McAdams and Shapiro, 2009). In *C. crescentus,* DnaA protein binds to DnaA boxes at the chromosome origin, initiating DNA replication by unwinding the DNA helix (Felletti et al., 2019). Its expression and activity are regulated by cell cycle factors like CtrA, ensuring timely replication. DnaA also ensures once-only chromosome replication and interacts with other cell cycle proteins, playing a multifunctional role in cell cycle regulation and progression. GcrA, a key transcriptional regulator, collaborates with cell cycle factors like CtrA to control DNA replication, chromosome segregation, and cell division in *C. crescentus* (Fioravanti et al., 2013). GcrA binds to gene promoters, acting as an activator or repressor, and regulates cell cycle-related genes. Its interaction with CtrA at different cell cycle stages finely tunes gene expression. GcrA also influences DnaA activity to time DNA replication accurately and regulates stalk formation and polar growth. It adapts the cell cycle and metabolism to environmental changes, forming a complex regulatory network essential for *C. crescentus* cell cycle precision. In *Sinorhizobium meliloti*, a model rhizobial strain closely related to *C. crescentus*, key cell cycle regulatory genes such as *ctrA, divJ, cpdR*, and *podJ* have been identified through homology analysis. These genes are crucial for cell division in rhizobia and also play a role in the development of symbiotic nodules (Xue and Biondi, 2019). In *S. meliloti*, CtrA is a key cell cycle regulator, controlling gene expression to influence replication, division, and morphogenesis (Pini et al., 2015; Schallies et al., 2015). Its activity is cell cycle-stage dependent, essential for a normal cycle. CtrA stability is regulated by cell cycle-controlled protein degradation, important for differentiation processes during nitrogen-fixing symbiosis. Although functionally similar to CtrA in *C. crescentus*, the *S. meliloti* CtrA regulates through different genes, like negatively regulating the Min system instead of directly controlling the Fts complex for cell division timing. In our previous study on the function of the NtrY/NtrX two-component system in *S. meliloti*, the phosphorylated NtrX protein directly activated the expression of *dnaA* and *ftsZ* genes, and repressed the expression of *ctrA* and *gcrA* genes, thereby regulating cell division (Xing et al., 2022). NtrX is a response regulator protein composed of a receiver domain and a DNA-binding domain. The receiver domain is responsible for sensing upstream signals, typically phosphorylation signals from histidine kinases, while the DNA-binding domain allows NtrX to bind to specific DNA sequences, thereby regulating gene expression (Xing et al., 2022; Fernandez et al., 2017). The receiver domain of NtrX contains a conserved phosphorylation site, usually an aspartate residue. NtrX regulates nitrogen metabolism and the expression of related genes in several bacteria, and plays a regulatory role in bacterial motility and succinoglycan production in *S. meliloti* (Wang et al., 2013; Calatrava-Morales et al., 2017)., it is an interesting question that the expression of cell cycle regulators is affected by HU homologs with acetylation to operate cell division in bacteria. In the present study, the stimulating mutants of the HU homolog of *S. meliloti* were created for investigation of cell division phenotypes and gene expression.

2. Materials and methods

2.1. Strains and medium

The bacterial strains employed in this study are detailed in Table S1. *E. coli* strains DH5a, MT616, and BL21 (DE3) were cultivated in LB medium at 37 °C, while *S. meliloti* strains were nurtured in LB/MC medium at 28 °C (Leigh et al., 1985). The study utilized following antibiotics at the specified concentrations: chloramphenicol at 10μg ml^{-1}, neomycin at 200μg ml^{-1}, kanamycin at 25μg ml^{-1}, gentamicin at 10μg ml^{-1}, tetracycline at 10 μg ml^{-1}, and streptomycin at 500 μg ml^{-1}.

2.2. Reconstruction of the three-dimensional (3D) structure of S. meliloti HupB protein

The amino acid sequence of the HupB protein was obtained from the *S. meliloti* 1021 genome website. Subsequently, a search for the 3D templates of the HupB protein was conducted on the Swiss-Model website. Utilizing the template with the highest identity, the 3D structure of *S. meliloti* HupB was reconstructed on the Swiss-Model website and then downloaded in PDB format. The HupB structure file was opened using PyMOL (https://www.schrodinger.com/) and transformed into a cartoon representation of its secondary structures. Lysine residues were identified, and the nearby negatively charged amino acids, such as aspartate and glutamate, were located. The measurement function between atoms was employed to determine the distance between oxygen and nitrogen atoms, which was followed by an evaluation of the potential for forming salt bridges.

2.3. Mass spectrometry analysis of acetyl modification sites in the HupB protein of S. meliloti

Urea buffer (8M Urea, 100 mM Tris/HCl, pH 8.5) was utilized for sample lysis and protein extraction. Protein quantification was performed using the Bradford Protein Assay Kit. DTT was added to each protein sample to a final concentration of 10 mM, followed by mixing at 600 rpm for 1.5 h at 37 °C and subsequent cooling to room temperature. IAA was then added to a final concentration of 50 mM, followed by incubation in the dark for 30 min. UA concentration was diluted to 2 M by adding 4 times the volume of 50 mM Tris–HCl (pH 8.0). Trypsin was added to the samples (trypsin: protein ratio 1:50), and the mixture was

incubated at 37 °C for 15–18 h TFA was added to a final concentration of 0.1 %, and the pH was adjusted to ≤3 using 10 % TFA. Digested peptides were desalted on C18 Cartridges (Empore™ SPE Cartridges C18 -standard density, bed I.D. 7 mm, volume 3 ml, Sigma) and lyophilized. Samples were reconstituted in 1.4 mL of precooled IAP Buffer, followed by the addition of pretreated Anti-Ac-K antibody beads (PTMScan Acetyl-Lysine Motif [Ac-K] Kit, Cell Signaling Technology) and incubation at 4 °C for 1.5 h The mixture was centrifuged at 2000 × *g* for 30 s, the supernatant was discarded, and the beads were washed thrice with 1 mL precooled IAP Buffer and precooled water, respectively. The washed beads were incubated with 40 μL of 0.15 % TFA for 10 min at room temperature, followed by another 40 μL of 0.15 % TFA and centrifugation at 2000 × *g* for 30 s to obtain the supernatant. The supernatant was desalted using C18 STAGE Tips and subjected to LC-MS/MS analysis on a Q Exactive HF/HFX mass spectrometer (Thermo Scientific) coupled to Easy nLC (Proxeon Biosystems, now Thermo Fisher Scientific) for 120 min. Peptides were loaded onto a reverse phase trap column (Thermo Scientific Acclaim PepMap100, 100 μm*2 cm, nanoViper C18) connected to a C18-reversed phase analytical column (Thermo Scientific Easy Column, 10 cm long, 75 μm inner diameter, 3 μm resin) in buffer A (0.1 % Formic acid) and separated with a linear gradient of buffer B (84 % acetonitrile and 0.1 % Formic acid) at a flow rate of 300 nl/min controlled by IntelliFlow technology. The mass spectrometer was operated in positive ion mode. MS data was acquired using a data-dependent top10 method by dynamically choosing the most abundant precursor ions from the survey scan (300–1800 *m/z*) for HCD fragmentation. The AGC target and maximum inject time were set to $3e^6$ and 10 ms, respectively. The dynamic exclusion duration was 40.0 s. Survey scans were acquired at a resolution of 70,000 at *m/z* 200, while the resolution for HCD spectra was set to 17,500 at *m/z* 200 and isolation width of 2 *m/z*. The normalized collision energy was 30 eV, while the underfill ratio was set to 0.1 %. The instrument was run under peptide recognition mode. MS raw data for each sample were combined for identification and quantitation analysis using MaxQuant software (Martinez-Val et al., 2017). The identification and quantitation indexes in MaxQuant are set as follows: Enzyme, trypsin; Max missed cleavages, 2; Main search (mass tolerance of precursor ions), 6 ppm; First search (mass tolerance of precursor ions), 20 ppm; MS/MS Tolerance (mass tolerance of MS2), 20 ppm; Fixed modifications, carbamidomethyl; Variable modifications, acetyl(K); Database, iant.toulouse.inra.fr/bacteria/annotation/cgi/rhime.cgi; Database pattern, reverse; Peptide FDR, ≤0.01; Site FDR, ≤0.01; Protein FDR, ≤0.01; Time window (match between runs), 2 min.

2.4. Construction of the *hupB* mutants of *S. meliloti*

Approximately 800 bp DNA sequences upstream and downstream of the *hupB* gene were selected as replacement fragments for homologous recombination. These flanking fragments were amplified using the high-fidelity Phanata Max DNA polymerase (Thermo Fisher Scientific), with Rm1021 genomic DNA as the template, and the PCR primers were listed in Table S2. The fragments were overlappingly amplified by PCR at a 1:1 ratio. The PCR product was purified and digested with *BamH*I and *Xba*I enzymes, yielding the purified product and vector pK18mobsacB (Schafer et al., 1994). The digested PCR products were ligated to the linear vectors using T4-DNA ligase, resulting in the gene-deleted plasmid pΔ*hupB*. pΔ*hupB* was introduced into the Rm1021/p*hupB* through tri-parental mating, and the transconjugants were selected on LB/MC agar plates containing streptomycin and neomycin. These transconjugants were streaked on fresh LB/MC/Sm/Nm agar plates and inoculated in 3 ml of LB/MC/Sm/Nm broth to determine the bacterial cell density. After incubation at 28 °C for 12–18 h, the bacterial cell density reached 0.8–1.0 at OD_{600}. Bacterial cells were collected by centrifugation at 8000 rpm for 1–2 min, resuspended in 1 ml of fresh LB/MC broth, and then diluted 10 times. Sixty μl of the diluted cells were spread on LB/MC/Sm agar plates with 10 % sucrose and incubated at 28 °C for 3–4 days. Single colonies were picked and streaked on LB/MC/Sm and LB/MC/Sm/Nm agar plates. Colonies sensitive to neomycin were used for PCR amplification and DNA sequencing to confirm the Δ*hupB*/p*hupB* mutant. The construction of the lysine-arginine and lysine-glycine substitutions in the HupB protein was achieved by introducing pΔ*hupB* into Rm1021/p$hupB^{3K\text{-}3R}$ and Rm1021/p$hupB^{3K\text{-}3G}$ via tri-parental mating, followed by similar steps as in the construction of Δ*hupB*/p*hupB* to obtain Δ*hupB*/p$hupB^{3K\text{-}3R}$ and Δ*hupB*/p$hupB^{3K\text{-}3G}$

2.5. Growth curve determination of *S. meliloti hupB* mutants

S. meliloti cells were selected from fresh prepared LB/MC plates and inoculated into 3 ml of LB/MC broth supplemented with appropriate antibiotics. The cultures were incubated overnight in a shaker incubator at 250 rpm/min and 28 °C. Subsequently, the cells were sub-cultured at a 1:50 ratio into 50 ml of LB/MC broth containing appropriate antibiotics. The optical density at 600 nm (OD_{600}) was monitored every 2 to 3 h using a visible spectrophotometer, and these measurements were utilized to construct a growth curve.

2.6. Morphology and cell length statistics of *S. meliloti hupB* mutants

The plasmid pHC60, which constitutively expresses GFP, was introduced into the wild-type and mutant strains of *S. meliloti*. The transconjugants were then cultured overnight in 5 ml LB/MC broth at 28 °C and 250 rpm/min. Subsequently, 500 μl of the overnight culture was used to 50 ml of fresh LB/MC broth for subculture. The bacteria were allowed to grow to the logarithmic phase (OD_{600}=0.8–1.0), after which 1 ml of the bacterial solution was aspirated and centrifuged at 6000 rpm for 3 min to pellet the cells. The cell pellet was then resuspended in 0.85 % sterile saline and centrifuged twice for further purification. The morphology of the bacterial cells was examined using a Zeiss fluorescence microscope (green fluorescence channel) with a 100 × objective lens of, and the cell images were captured using the ZEN software. The cell area was measured using Image J software and converted to cell length, assuming an average cell width of 1 μm). Approximately 1000 cells were counted for each type, with those exceeding 1 μm in width being considered valid data. A frequency distribution table was compiled, and the data underwent *t*-test for statistical analysis. Significant differences between groups are denoted as follows: * for $P < 0.05$, ** for $P < 0.01$), and *** for $P < 0.001$.

2.7. RNA-seq and bioinformatic analysis

A cell pellet of *S. meliloti* was initially prepared by centrifuging 20 ml of overnight culture at 6000 rpm for 5 min at 4 °C. The cell pellet was subsequently washed twice with DEPC-treated water, resuspended in 200 μl of DEPC water, and frozen in liquid nitrogen. The frozen cells were ground into powder in an EP tube using an electronic mortar, followed by RNA extraction with Trizol (life technology). RNA-seq and bioinformatic analyses were conducted by Sinotech Genomics, Shanghai. For specific experimental procedures, please refer to the documents available on the company's website.

2.8. qRT-PCR and qPCR analysis

RNA reverse transcription was conducted using the PrimeScript RT reagent Kit with gDNA Eraser (TAKARA). The qPCR and qPCR reaction setup were based on a previously established method (Tang et al., 2017). SMc00128 was employed as the internal reference gene for quantifying the gene expression level. All PCR primers were listed in Table S2.

2.9. Protein expression, purification, and immunoblotting

E. coli BL21 cells harboring the plasmid with *hupB* or its mutants were cultured overnight in 5 ml LB broth supplemented with ampicillin in an incubator shaker set at 37 °C and 250 rpm/min. The entire

bacterial cell culture was then transferred into 100 ml of fresh LB broth and incubated for 12 h at 37 °C. IPTG (0.5 mM) was then added to the broth for induction, and the culture was incubated in an incubator shaker set at 18 °C and 250 rpm/min for 8 h The His-tag fusion protein purification was then carried out using Ni^{2+}affinity chromatography system according to a previously established protocol (Tang et al., 2017). The elutes were analyzed by SDS/PAGE to assess protein binding. The purified HupB fusion protein was successfully prepared and used to generate rabbit anti-polyclonal antibodies at Hangzhou Hua'an Biotechnology Co., Ltd, followed by immunoblotting analysis (Tang et al., 2017). The assays utilized polyclonal antibodies of anti-NtrX, anti-CtrA, anti-GcrA, and anti-DnaA (Xing et al., 2022).

2.10. Chromatin immunoprecipitation dna sequencing (ChIP-seq) analysis

High-throughput sequencing, data processing, RNA sequence, and ChIP sequence analyses were conducted by Shanghai Bioer Bioengineering Ltd. Each sample yielded 2 G of sequencing data was, with over 90 % of bases having a quality score higher than 20 (Q20). The data underwent initial preprocessing, followed by the removal of small RNA and rRNA using the SeqTK method, resulting in clean reads that comprised >95 % of the original data. Bowtie2 (version: 2–2.0.5) was chosen for genome mapping of the preprocessed reads due to its suitability for prokaryotic transcriptome sequencing data. The genome database used was *S. meliloti* 1021, with mapping ratios ranged from 92 % to 98 %. Reads were converted into FPKM (Fragments Per Kilobase of exon model per Million mapped reads) for gene expression normalization. The number of fragments per gene was counted using the HTSeq bowtie2 tool, normalized with the TMM (trimmed mean of M values) method, and calculated using a Perl script to obtain the FPKM value of each gene.

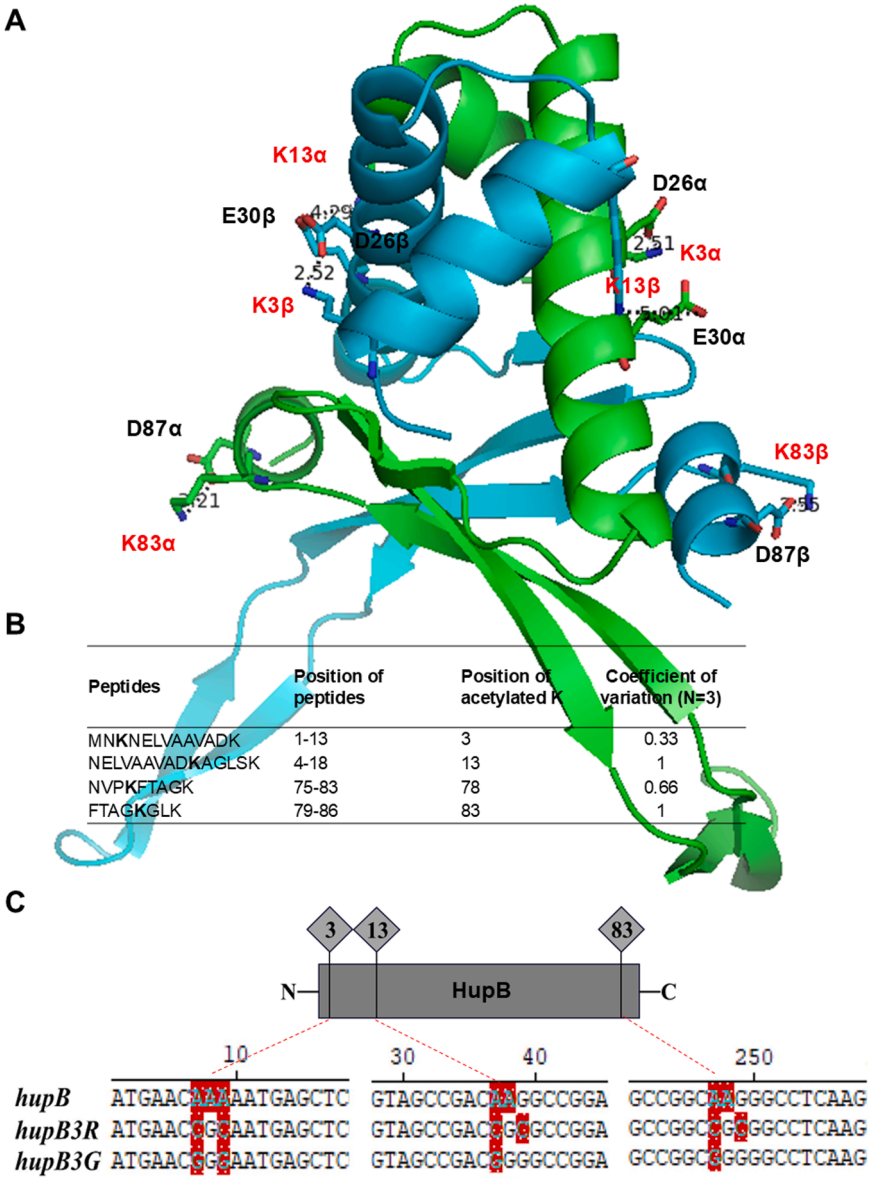

Peptides	Position of peptides	Position of acetylated K	Coefficient of variation (N=3)
MN**K**NELVAAVADK	1-13	3	0.33
NELVAAVAD**K**AGLSK	4-18	13	1
NVP**K**FTAG**K**	75-83	78	0.66
FTAG**K**GLK	79-86	83	1

Fig. 1. Identification of acetylated lysine residues in the HupB protein from *S. meliloti*. A. 3D-structure reconstruction of HupB dimers from *S. meliloti*. K3α, the third lysine residue on subunit α; 2.51, the minimum distance between the carboxyl oxygen atom at position D26 on subunit a and the ε-amino nitrogen atom at position K3 on the same subunit (2.51 Å). **B.** Peptides containing acetylated lysine residues identified through high-resolution mass spectrometry analysis. Coefficient of Variation, the number of times peptides with acetyl-modified K were detected divided by the total number of detections. **C.** Mutations were introduced in the three key lysine residues of HupB in *S. meliloti*. *hupB,* a deletion mutant of *hupB* was generated in the chromosome following the expression of the IPTG-induced *hupB* gene from a plasmid (Δ*hupB*/p*hupB*); *hupB3R*, Δ*hupB*/p$hupB^{K3,\ 13,\ 83\ R}$; *hupB3 G*, Δ*hupB*/p$hupB^{K3,\ 13,\ 83\ G}$.

2.11. Electrophoretic mobility shift assay (EMSA)

A 30-bp oligonucleotide from the *dnaA* promoter was utilized as a probe to bind the purified HupB and its amino acid-substituted variants. The promoter was synthesized by Shanghai Sangon Biotech Co., Ltd. EMSA was conducted using the LightShift chemiluminescent EMSA kit (Thermo Scientific), following a previously described protocol (Xing et al., 2022).

3. Results

3.1. Lysine residues in HupB from S. meliloti are subject to differential acetylation modifications

The histone-like protein HupB, encoded by SMc01906 in *S. meliloti* 1021, comprises 90 amino acids, including 8 lysine residues (K3, K13, K18, K37, K59, K78, K83, and K86). HupB shares 34–41 % amino acid sequence identity with integration host factors HimA and IHFB. Classified as a basic DNA-binding protein, HupB also contains 5 arginine, 6 aspartate, and 2 glutamate residues. The 3-D model, generated via the Swiss model website suggests a dimer composed of 3 α-helix (two located in the C-terminus) and 5 β-fold sheets. The dimer had a 46.67 % identity with *Staphylococcus aureus* Hu protein, 8hd5.1(www.ncbi.nlm.nih.gov/Structure/pdb/8HD5), and boasts a 0.89 QEME (Quality Evaluation of Model and Experiment) score of 0.89 and QSQE (Quality of Structural Ensemble) score of 0.98. PyMOL analysis reveals that within a single subunit of the HupB protein dimer, two salt bridges are formed: K3-D26 (distance between N and O atoms: 2.51 Å and 2.52 Å) and K83-D87 (distance between N and O atoms: 3.55 Å and 3.21 Å). Additionally, there may be a weak salt bridge formed between the two subunits at K13-E30 (distance between N and O atoms: 4.29 Å and 5.01 Å), indicating that K3, K13, and K83 might be key residues for the protein's function (Fig. 1A). High-resolution mass spectrometry analysis of the pan-acetyl-Lysine immunoprecipitation products revealed that four peptide segments were detected across three independent experiments (Fig. 1B). Peptides with acetyl modifications on K13 and K83 were consistently detected, while the peptide with acetyl modification on K78 was observed in two experiments (Fig. 1B). The peptide with acetyl modification on K3 was only detected in one experiment, and the signal intensity was close to the detection limit (Fig. 1B). These results indicate that the acetyl modifications on these lysine residues are indeed present. We aimed to construct triple lysine substitution mutants (*hupB*$^{K3,13,\ 83R}$ and *hupB*^{K3,13,83Q}) to mimic the non-acetylated and acetylated states of HupB, based on the integrated analysis of structural and mass spectrometry data. However, base substitutions in the HupB-encoding gene within the genome proved unattainable. We could only delete the *hupB* gene in the genome and express the mutated gene from the plasmid pSRK-Gm. DNA sequencing confirmed that only one of the two planned mutant, *hupB*$^{3K\text{-}3R}$ (simulating the non-acetylated state), and *hupB*$^{3K\text{-}3G}$ (*hupB*$^{K3,13,\ 83G}$) were successfully constructed inadvertently, while *hupB*$^{3K\text{-}3Q}$ (simulating the acetylated state) was not (Fig. 1C).

3.2. HupB lysine substitutions lead to deficiencies in cell division in S. meliloti

We successfully constructed three *S. meliloti* strains (Δ*hupB/phupB*, Δ*hupB/phupB*$^{3K\text{-}3R}$, and Δ*hupB/phupB*$^{3K\text{-}3G}$) for analysis of cell growth and duplication. Δ*hupB/phupB*$^{3K\text{-}3G}$ exhibited faster growth than Δ*hupB/phupB*, while Δ*hupB/phupB*$^{3K\text{-}3R}$ showed slowest growth (Fig. 2A), indicating that acetylation of lysine residues in HupB affected the growth and duplication of *S. meliloti*. Cell morphology was assessed after introducing a constitutively expressing *gfp* gene. Notably, Δ*hupB/phupB*$^{3K\text{-}3R}$ culture contained numerous large abnormal cells (Fig 2E) and Δ*hupB/phupB*$^{3K\text{-}3G}$ culture had many small irregular cells (Fig 2F), compared to Δ*hupB/phupB* (Fig. 2D). These findings suggest that lysine acetylation in HupB influenced cell division in *S. meliloti*. The average

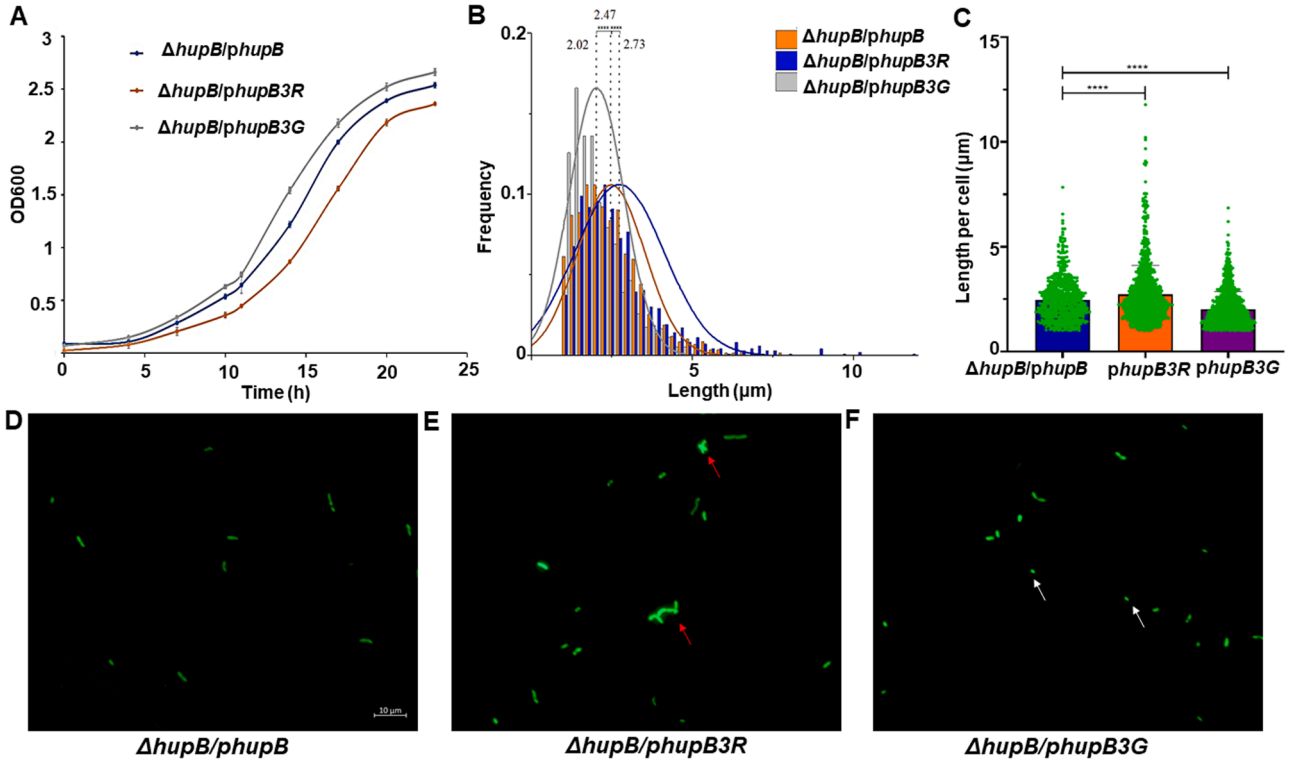

Fig. 2. HupB lysine substitutions mimic acetylated and non-acetylated affect *S. meliloti* cell division. A. Growth curves of Δ*hupB/phupB* with lysine substitutions. **B-C.** Analysis of cell length measurements in Δ*hupB/phupB* with lysine substitutions. Statistical analysis was performed using Student's *t*-tests; **** denote $P < 0.001$; 2.47, the average length of the cells. **D-F.** Cell morphology of Δ*hupB/phupB* with lysine substitutions. Abnormal cells are indicated using arrows; bars, 10 μm.

cell lengths of Δ*hupB*/p*hupB*, Δ*hupB*/p*hupB*$^{3K\text{-}3G}$, and Δ*hupB*/p*hupB*$^{3K\text{-}3R}$ were 2.47 μm, 2.02 μm, and 2.73 μm, respectively (Fig 2B). Δ*hupB*/p*hupB*$^{3K\text{-}3R}$ culture had longer cells, while the Δ*hupB*/p*hupB*$^{3K\text{-}3G}$ culture had shorter cells (Fig. 2C). These results suggest that non-acetylated HupB prevented cell division, while acetylated protein promoted it.

3.3. HupB lysine substitutions activated transcription of cell cycle regulator genes

To understand how the acetylation of lysine residues on the HupB protein influences cell division in *S. meliloti*, we investigated the differential expression of cell cycle-related genes. RNA-Seq analysis revealed that 166 genes were differentially expressed in the Δ*hupB*/p*hupB*$^{3K\text{-}3R}$ mutant compared to the Δ*hupB*/p*hupB* strain (Fig. 3A, Table S3), with 129 genes being downregulated and 37 genes upregulated. Similarly, 777 genes showed differential expression in the Δ*hupB*/p*hupB*$^{3K\text{-}3G}$ mutant, with 271 genes downregulated and 506 genes upregulated (Fig. 3A, Table S3). Of these, 39 genes were differentially expressed in both mutants: 19 were upregulated and 20 were downregulated (Fig. 3A). The data indicate that the *hupB*$^{3K\text{-}3G}$ mutation results in a greater impact on gene expression than the *hupB*$^{3K\text{-}3R}$ mutation, with the former leading to the up-regulation of more genes and the latter to the down-regulation of more genes.

Transcriptomic analysis further revealed that the cell cycle regulatory genes *minCDE, ftsZ1*, and *ftsZ2* were slightly upregulated in the *hupB*$^{3K\text{-}3R}$ mutant compared to the non-mutation strain, while *gcrA, ctrA, dnaA*, and *ccrM* showed slightly increased expression in the *hupB*$^{3K\text{-}3G}$ mutant (Fig. 3B).

To validate these findings, total RNA was extracted from the rhizobial cells under identical conditions and analyzed using quantitative RT-PCR. The results confirmed similar levels of *hupB* expression across the three strains (Fig. 3C). The transcripts of *ctrA, gcrA, dnaA*, and *ntrX* were found to be higher in both substitution mutants compared to the non-mutation strain (Fig. 3C), with the *hupB*$^{3K\text{-}3G}$ mutant exhibiting higher transcription levels than the *hupB*$^{3K\text{-}3R}$ mutant (Fig. 3C). These data suggest that HupB$^{3K\text{-}3G}$ is more effective in promoting gene transcription than HupB$^{3K\text{-}3R}$.

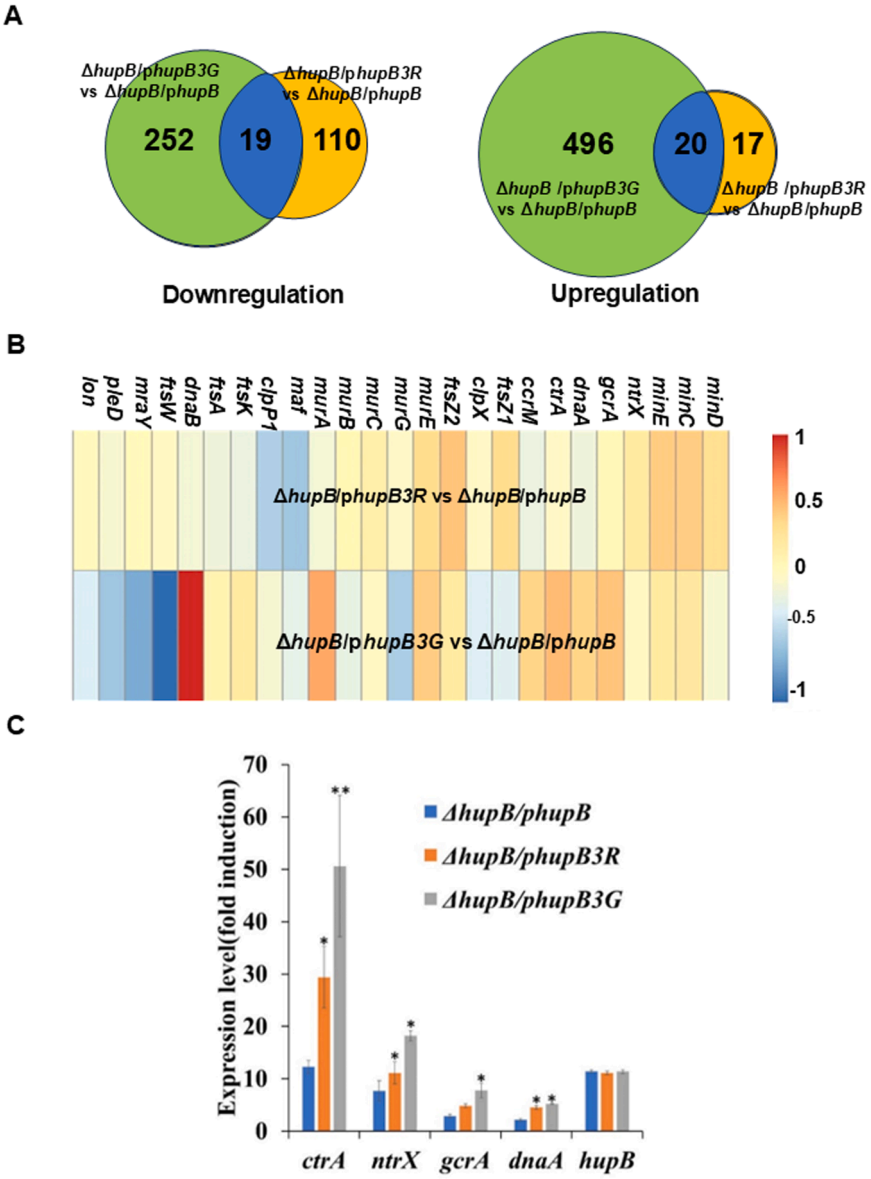

Fig. 3. Transcriptional activation of key cell cycle regulatory genes in *S. meliloti* HupB lysine substitution cells. A. Analysis of differential expression genes in HupB lysine substitution mutants through transcriptome (RNA-seq). **B-C.** Transcriptional upregulation of cell cycle regulatory genes determined by RNA-seq (B) and qRT-PCR (C). Statistical analysis was performed using Student's *t*-tests; ** denotes $P < 0.001$; * indicates $P < 0.05$.

3.4. HupB lysine substitutions cause differential expression of cell cycle regulator proteins

The transcriptional outcomes of cell cycle regulatory genes failed to account for the cellular growth and division phenotypes resulting from the mutation of Lys to Arg and Gly in HupB. Consequently, we hypothesized that there might be variations in protein expression levels. To test this hypothesis, we extracted total protein from rhizobia cells and conducted immunoblot analysis. Our findings revealed that in the Δ*hupB*/p*hupB*$^{3K\text{-}3R}$ cells, there was an increase in CtrA levels, while GcrA and DnaA levels decreased (Fig. 4A-B). Conversely, in the Δ*hupB*/p*hupB*$^{3K\text{-}3G}$ cells, CtrA levels significantly decreased, with a notable increase in GcrA and DnaA levels (Fig. 4A-B). These data suggest that the substitution of Lys with Arg and Gly in HupB resulted in opposing trends in the protein levels of CtrA, GcrA, and DnaA.

3.5. HupB with lysine substitutions exhibits differential patterns of genomic DNA binding

The homologous protein HupB is known to bind genomic DNA in various bacterial cells (Prieto et al., 2012; Liao et al., 2017). *In vitro* studies have demonstrated that acetylation of lysine residues in HupB can influence its DNA binding capacity (Holowka et al., 2017). However, it has remained unclear whether HupB with specific lysine substitutions in *S. meliloti* exhibits differential binding across the entire genome. Utilizing Chromatin Immunoprecipitation-DNA sequencing (ChIP-Seq) technology, this study reveals that HupB and its mutant variants display varying binding affinities towards the three replicons of the *S. meliloti* genome, with the order of preference being chromosome > pSymB > pSymA (Fig. 5A). Moreover, their binding tendency towards the DNA at the replicon ends is stronger compared to the middle regions (Fig. 5A). HupB$^{3K\text{-}3R}$ binds to a greater number of DNA fragments and longer segments than both HupB and HupB$^{3K\text{-}3G}$, with HupB$^{3K\text{-}3G}$ showing the least binding to the shortest fragments (Fig. 5B). The details are as follows: Δ*hupB*/p*hupB* cells yielded a total of 573 DNA fragments, ranging in length from 236 to 10,915 bp, while Δ*hupB*/p*hupB*$^{3K\text{-}3R}$ cells produced 1116 fragments, ranging from 240 to 11,124 bp (Table S4). Δ*hupB*/p*hupB*$^{3K\text{-}3G}$ cells, on the other hand, yielded 358 fragments, ranging from 248 to 5864 bp (Table S4). Predictions of the genomic DNA cis-elements targeted by HupB and its mutants reveal that HupB can bind to the highest number of these elements [36], with HupB3K-3R intermediate (Xue and Biondi, 2019), and HupB3K-3 G the lowest (Micka and Marahiel, 1992) (Fig. 5C). These findings suggest that lysine substitutions in the HupB protein modulate its binding pattern to the *S. meliloti* genome.

3.6. HupB proteins with lysine substitutions differentially bind to DNA fragments from cell cycle regulatory genes

Analysis of the ChIP-seq data revealed differential precipitation of DNA fragments from cell cycle regulatory genes by the antibody in the presence of HupB and its mutants (Fig 6A). Notably, *ctrA* gene fragments were slightly more abundant in *hupB*$^{3K\text{-}3R}$ cells compared to the wild-type *hupB* cells, whereas in *hupB*$^{3K\text{-}3G}$ cells, they were drastically reduced; *dnaA* gene fragments showed a significant decrease in both *hupB* mutant cells; and *gcrA* gene fragments also decreased, with a more pronounced reduction in *hupB*$^{3K\text{-}3G}$ cells (Fig. 6A).

To confirm these findings, we performed a ChIP-PCR experiment under identical conditions. The results indicated that the precipitation of the *ctrA* gene promoter region was inclined to increase in *hupB*$^{3K\text{-}3R}$ cells, while displaying an opposite trend in *hupB*$^{3K\text{-}3G}$ cells; the promoter regions of *dnaA* and *gcrA* genes exhibited a significant decrease in both *hupB* mutant cells (Fig. 6B). This outcome aligns closely with the ChIP-seq data, suggesting that lysine substitution mutations in HupB, whether they mimic acetylation or not, can influence its binding to the promoter regions of cell cycle regulatory genes.

Wild-type HupB and its lysine-substituted variants were expressed and purified. A DNA fragment rich in A/T from the *dnaA* promoter was synthesized and used as a probe for gel shift assays. The assay results demonstrated that HupB and the HupB$^{3K\text{-}3R}$ mutant proteins formed larger protein-DNA complexes upon interaction with the probe, whereas the HupB$^{3K\text{-}3G}$ mutant protein formed smaller complexes (Fig. 6C). Quantitative analysis of the HupB-DNA complex bands using Image J reveals that the amount of DNA complex formed by HupB and HupB3$^{K\text{-}3R}$ is greater than that formed by HupB$^{3K\text{-}3G}$ (Fig. 6D). These findings imply that non-acetylated proteins have a higher binding density to DNA, while acetylated proteins exhibit reduced binding to the target DNA.

3.7 Lysine substitutions potentially alter the conformation of the DNA-binding HupB protein

Using the 3D structure of HU protein from *S. aureus* bound to a DNA fragment (4qju) as a templat (Kim et al., 2014), the 3D structures of *S. meliloti* HupB and its mutants were reconstructed. The distances between the K and D/E nitrogen and oxygen atoms were then measured

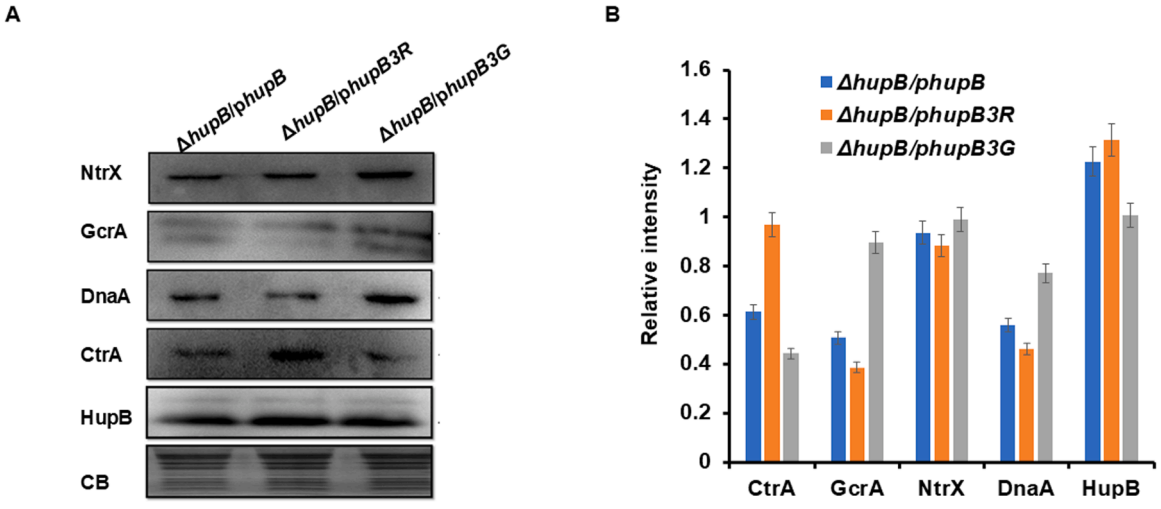

Fig. 4. Protein of key cell cycle regulators expressed in *S. meliloti* HupB substitutions. A, Immunoblotting; CB, Coomassie brilliant blue staining showing some of the protein bands. B, Quantitative assess of the immunoblotting data with Image J. Relative intensity, the signal intensity of the Western blot band divided by the intensity of the strongest band in Coomassie brilliant blue staining.

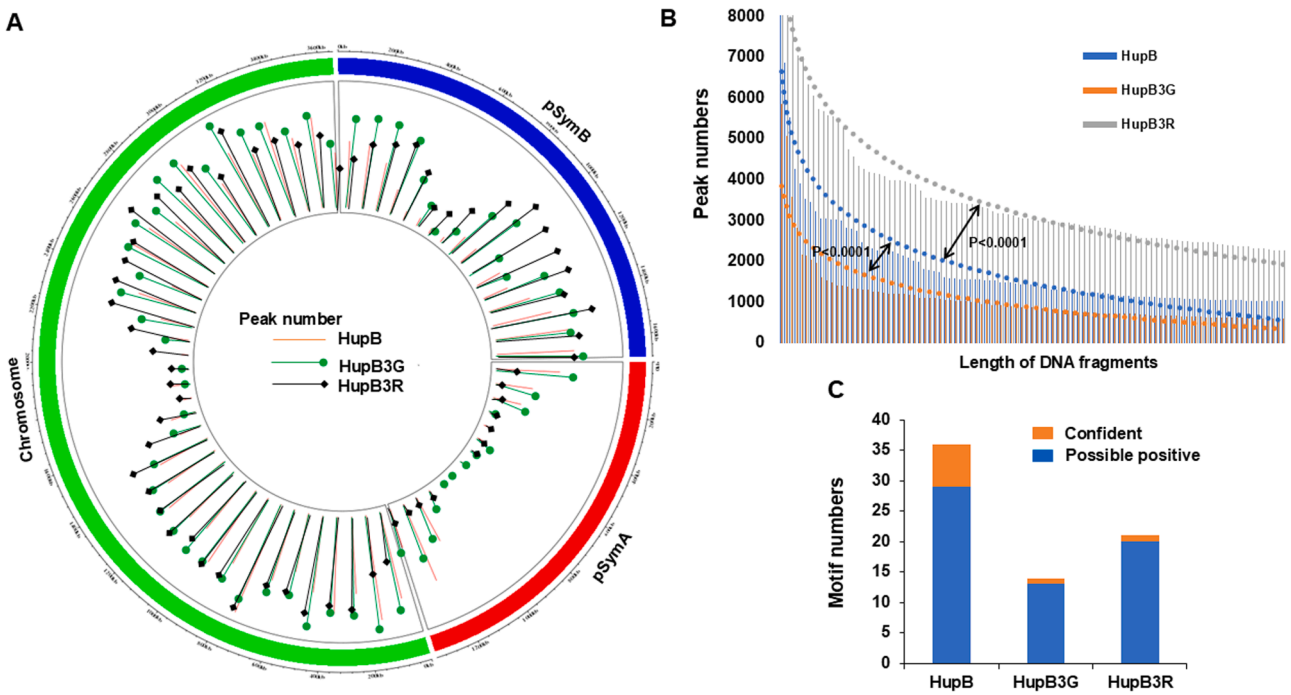

Fig. 5. *S. meliloti* genomic DNA binding features of HupB lysine substitutions. A. Distribution of genomic DNA fragments precipitated from ChIP-seq assays. B. Statistical analysis of genomic DNA fragments precipitated from *S. meliloti* cells. Student's *t*-tests were used here. C. DNA binding motifs in the genome by HupB and its substitutions.

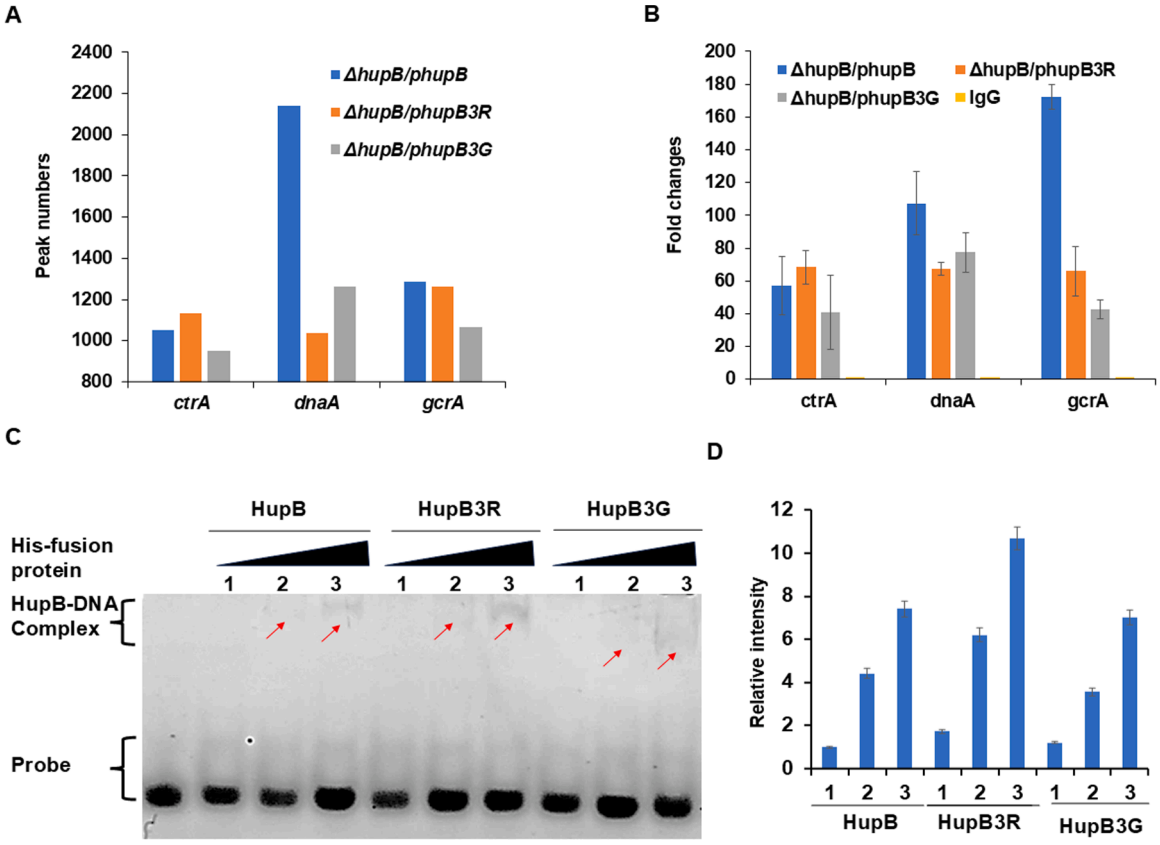

Fig. 6. Cell cycle regulatory gene fragments recognized by HupB and its substitutions. A. Enriched DNA fragments of cell cycle regulatory genes obtained via ChIP-seq. **B**. Promoter fragments of key cell cycle regulatory genes precipitated from ChIP-PCR assay. Statistical analysis was performed using ANOVA. **C.** Binding of HupB and its K substitutions to the promoter fragment of *dnaA* based on the Electrophoretic Mobility Shift Assay (EMSA). **D**. Quantitative analysis of the HupB-DNA complex levels was performed using Image J software. 1–3 correspond to the concentrations of three HupB and its mutant proteins from low to high (C-D).

using PyMOL software to analyze the strength of the salt bridge interactions. We found that, compared to the 3D structure reconstructed using the unbound DNA template 8hd5, after DNA binding, the distance between the side chain nitrogen and oxygen atoms of K83-D87 on subunit α was shortened (from 3.21 Å to 2.54 Å), while the distance between the side chain nitrogen and oxygen atoms of this residue pair on subunit β increased (from 2.55 Å to 3.5 Å; Fig. 1A and 7A). The distance between the side chain nitrogen and oxygen atoms of K3-D26 on both

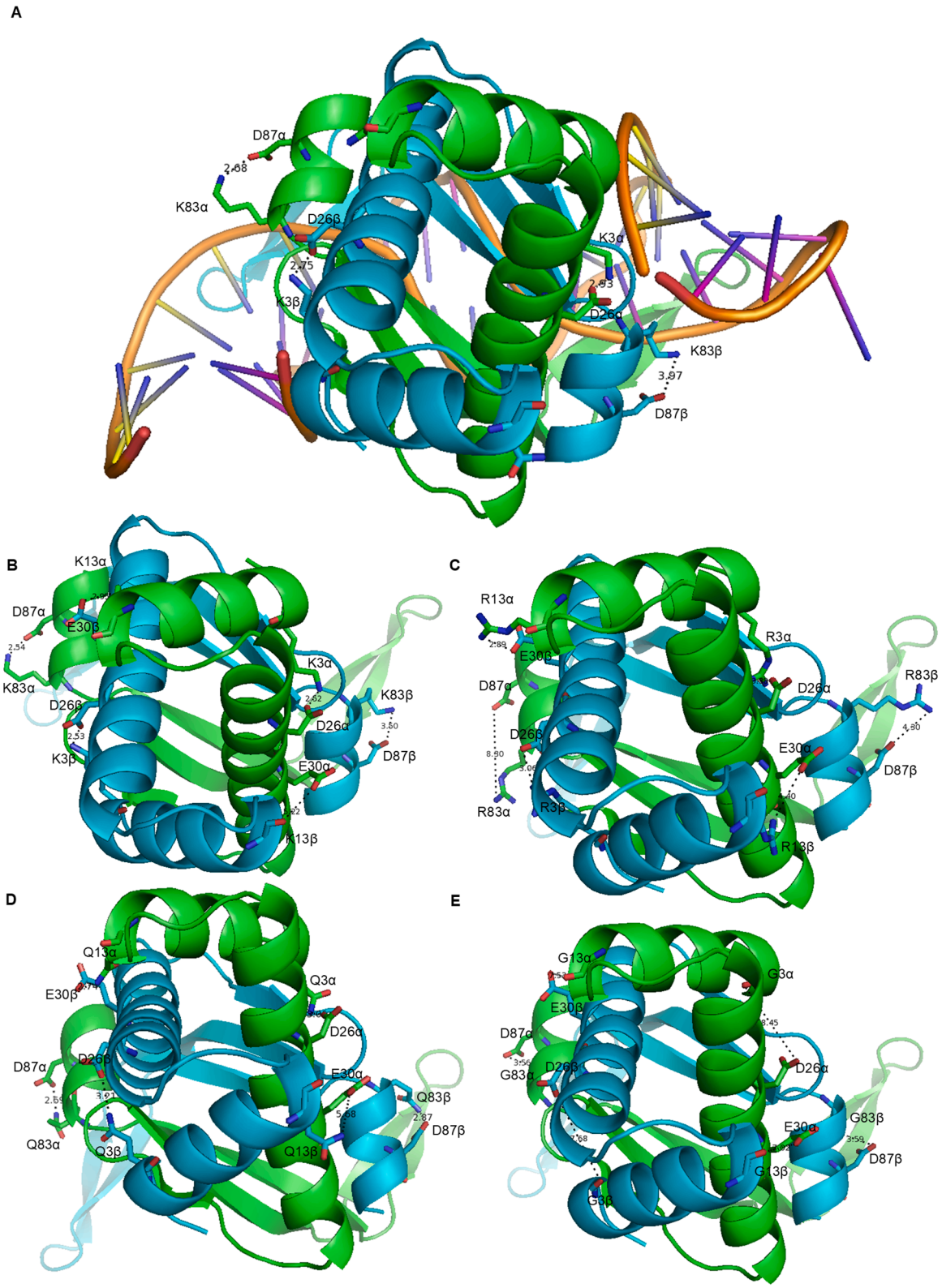

Fig. 7. 3D structures of *S. meliloti* HupB and its substitutions bound to DNA. 3D structure of HU-DNA complex from *S. aureus* (4qju). **B-E**. Stimulated 3D structures of HupB (**B**), HupB$^{3K\text{-}3R}$ (**C**) and HupB$^{3K\text{-}3Q}$ (**D**) HupB$^{3K\text{-}3G}$ (**E**) were present. D87α, the 87th residue on the α subunit is aspartic acid; 2.68, the distance between the nitrogen and oxygen atoms is 2.68 Å

subunits did not change significantly (Fig. 1A and 7A). These data indicate that after DNA binding, the salt bridges at the C-terminus (involved in DNA binding) of the HupB protein subunits underwent asymmetric changes. Additionally, the distance between the side chain nitrogen and oxygen atoms of K13-E30 across the two subunits also underwent asymmetric changes (from 4.29 Å to 2.95 Å; 5.01 Å to 5.22 Å; Fig. 1A and 7A), suggesting that DNA binding led to asymmetric alterations in the interactions between the HupB protein subunits.

Mutating the three K residues on the HupB protein to R resulted in an increase in the distance between the side chain nitrogen and oxygen atoms of K3-D26 and K83-D87 within both subunits (from 2.52 Å to 3.88 Å; 2.53 Å to 3.06 Å; 2.54 Å to 8.3 Å; 3.5 Å to 4.3 Å), while the distance between the side chain nitrogen and oxygen atoms of K13-E30 across the two subunits decreased (from 2.95 Å to 2.89 Å; 5.22 Å to 4.4 Å; Fig. 7B). This indicates that after the substitution mutation, the electrostatic interactions within the subunits and between the subunits underwent opposite changes, meaning the attraction between the charged groups within the subunits decreased, while the attraction between the subunits increased. Mutating the three K residues on the HupB protein to G resulted in an increase in the distance between the side chain nitrogen and oxygen atoms for both the intra-subunit K3-D26 and K83-D87 and the inter-subunit K13-E30 (from 2.52 Å to 8.45 Å; 2.53 Å to 7.68 Å; 2.54 Å to 3.56 Å; 3.5 Å to 3.59 Å; 2.95 Å to 7.53 Å; 5.22 Å to 7.02 Å; Fig. 7D). This indicates that after the substitution mutation, the electrostatic interactions within the subunits and between the subunits disappeared, leading to a relaxed conformation of the protein. Mutating the three K residues on the HupB protein to Q resulted in an increase in the distance between the side chain nitrogen and oxygen atoms for both K3-D26 and K83-D87 within the alpha subunit (from 2.52 Å to 3.06 Å and 2.54 Å to 2.69 Å), while within the beta subunit, the distance between the side chain nitrogen and oxygen atoms of K3-D26 and K83-D87 increased for one and decreased for the other (from 2.53 Å to 3.21 Å; 3.5 Å to 2.87 Å). The changes in the distance between the side chain nitrogen and oxygen atoms of K13-E30 across the two subunits were similar to those within the beta subunit (from 2.95 Å to 2.74 Å; 5.22 Å to 5.68 Å; Fig. 7C). Through the above structural simulation analysis, it was found that after the HupB protein binds to DNA, its conformation may undergo significant changes; when the three Lysine residues on it are replaced by Arginine, Glycine, and Glutamine, respectively, the conformational changes of the protein are each different.

4. Discussion

The acetylation of histone-like protein HU can modulate DNA compaction, replication, and gene expression in bacteria (Prieto et al., 2012; Stojkova et al., 2019; Liao et al., 2017; Kohler and Marahiel, 1997). However, the role of HU protein acetylation in regulating cell division in bacterial cells is seldom documented, and its underlying regulatory mechanism remains largely elusive. In this study, we employed molecular genetic approaches to successfully generate mutants of the HU homologous protein HupB in *S. meliloti,* by substituting three lysine (K) residues with arginine (R) and glycine (G), mimicking acetylated and non-acetylated states, respectively. For the first time, we observed that these two mutants exhibited nearly opposite phenotypes in cell division. We further elucidated the potential mechanisms of action by analyzing the differences in HupB's DNA binding affinity, the altered expression of cell cycle regulatory proteins, and their direct modulation (Fig. 8).

It has been reported in various bacterial species that several K residues on HU homologous proteins can undergo acetylation (Kano et al., 1985; Liao et al., 2017; Micka and Marahiel, 1992). Utilizing high-resolution proteomics, we identified four K residues on *S. meliloti*'s HupB that are candidates for acetylation modifications. Given that 3D structural analysis suggested that three of these (K3, K13, and K83) could potentially form salt bridges, which are likely crucial functional sites, and K78 might directly interact with DNA, we decided to mutate these three residues simultaneously (Fig. 1). We avoided single amino acid residue replacement mutations due to concerns that such mutants might not display discernible genetic phenotypes. In future research, we intend to perform replacement mutations on individual K residues to ascertain if there exists a critical modification site.

The *hupB* gene in *S. meliloti*, similar to its counterpart in *B. subtilis*, is vital for growth and reproduction (Micka and Marahiel, 1992). Consequently, we were unable to successfully screen for deletion mutants of this gene and substitution mutants of the three lysine residues in the *hupB* gene within the genome. Despite successfully constructing three conditional knockout strains—Δ*hupB*/p*hupB*, Δ*hupB*/p*hupB*$^{3K\text{-}3R}$, and Δ*hupB*/*hupB*$^{3K\text{-}3G}$ (Fig. 1C), —we were unable to obtain the Δ*hupB*/*hupB*$^{3K\text{-}3Q}$ mutant. The likely explanation is that mutating the three lysine residues on HupB to glutamine (Q) may result in abnormal protein structure and function, which adversely affects the survival of *S. meliloti* cells, potentially differing from the effects observed in *B. subtilis*. This hypothesis is also supported by the results of 3D structural simulation analysis of the mutant protein (Fig. 7).

We suggest that the HupB$^{3K\text{-}3G}$ mutation can mimic the acetylated state of HupB. Firstly, this mutant displays cellular phenotypes that are nearly opposite to those of HupB$^{3K\text{-}3R}$ cells (Fig. 2). Secondly, the expression patterns of key cell cycle regulatory proteins are largely

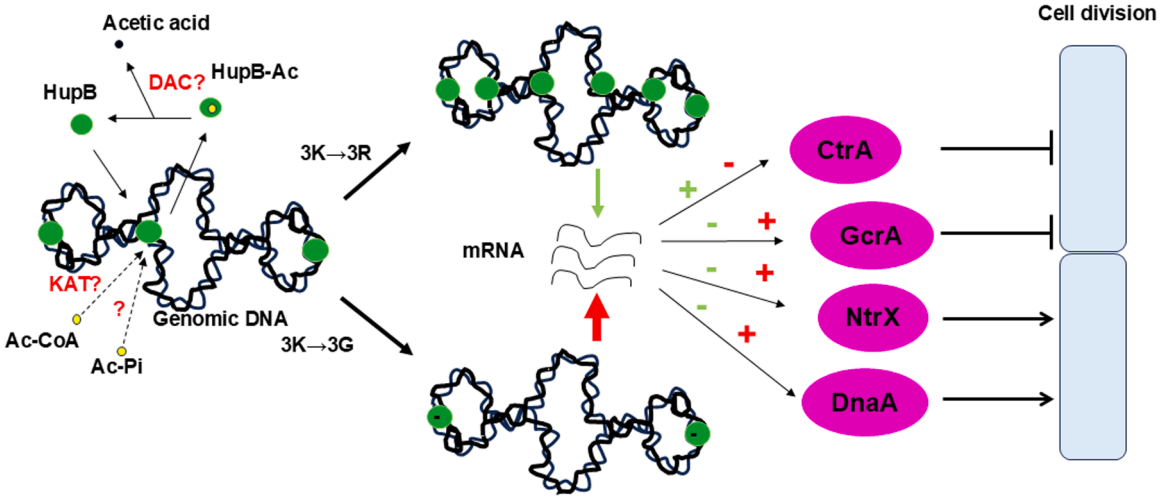

Fig. 8. Model of HupB modified by acetylation to regulate cell division. Ac-Co, acetyl-CoA; Ac-Pi, acetyl phosphate; HupB-Ac, acetylated HupB; + or arrows, promotion or positive regulation.

converse between these mutants (Fig. 4). Moreover, the DNA binding patterns and capacities are either opposite or distinct (Fig. 5-6). Lastly, 3D structural simulations under the DNA-bound state reveal profoundly different protein conformations (Fig. 7). We contend that the role of acetylation on the lysine residues of the HupB protein is to neutralize positive charges and disrupt salt bridges, thereby altering the conformation and function of the protein. Consequently, mutations to arginine (R) and glycine (G) exhibit opposing phenotypes or effects. We attempted to elucidate the cell division defect phenotypes of the HupB lysine substitution mutants (Fig. 2) by examining changes in the expression of cell cycle regulatory proteins. These phenotypes may arise from the differential expression of cell cycle regulators (CtrA, GcrA, DnaA, and NtrX) (Fig. 4). Interestingly, transcriptional analysis revealed significantly elevated mRNA levels for these key cell cycle regulatory genes in the two hupB mutants (Fig. 3), which were not entirely consistent with their protein expression levels (Fig. 4). Our interpretation is that the expression of these genes in the context of HupB mutations may not be solely governed by transcriptional regulation but may also be subject to post-translational control.

The lysine substitution mutations in the HupB protein profoundly altered its binding affinity for genomic DNA fragments (Fig. 5A-B), aligning with findings on HU proteins with simulated acetylation modifications and unmodified forms in other strains (Köhler and Marahiel, 1998). However, we uniquely identified that HupB exhibits varying affinities towards the three replicons in the genome and different regions within the same replicon (Fig. 5A). Moreover, its lysine substitution mutations modified the originally identified DNA cis-elements (Fig. 5C), potentially stemming from alterations in protein conformation (Fig. 7).

Initially, we postulated that replacing lysine (K) residues in HupB with arginine (R), to mimic a non-acetylated state, might reinforce or sustain the salt bridges within the protein molecule. However, structural simulations of the DNA-bound HupB protein revealed unexpected alterations in electrostatic interactions both within and between subunits (Fig. 7C). Notably, the subunits adopted a more relaxed conformation internally, while the interactions between subunits intensified. This relaxed conformation at the C-terminus facilitates stronger electrostatic interactions between the positively charged amino acid residues of the protein and the phosphate groups on the DNA backbone, accounting for the enhanced affinity of the $HupB^{3K\text{-}3R}$ mutant for DNA fragments. Conversely, when K is substituted with glycine (G), the electrostatic interactions within and between the HupB mutant molecules are abolished, resulting in an overall more relaxed protein conformation (Fig. 7E) and impaired DNA binding (Fig. 5-6), thereby alleviating the inhibitory effect of HupB binding on gene expression (Fig. 3). The conformational changes induced by K replacement with glutamine (Q) are more nuanced (Fig. 7D), as glutamine is polar and may form new hydrogen bonds, complicating its interpretation as a simple mimic of lysine acetylation.

In conclusion, the HupB protein in *S. meliloti* undergoes acetylation modifications that modulate its conformation, influencing DNA binding and regulating the expression of cell cycle-related genes in an intricate fashion to govern cell division (Fig. 8). This work lays the groundwork for a more profound understanding of the regulatory mechanisms underlying bacterial cell division. However, the post-translational mechanisms by which the HupB protein orchestrates the differential expression of cell cycle proteins warrant further exploration.

Author statement

The authors listed on this manuscript confirm that the work reported is original, has not been published before and is not currently being considered for publication elsewhere. The manuscript has been read and approved by all named authors and that there are no other persons who satisfied the criteria for authorship but are not listed. We further confirm that the order of authors listed in the manuscript has been approved by all of us. We understand that the Corresponding Author is the sole contact for the Editorial process. He is responsible for communicating with the other authors about progress, submissions of revisions and final approval of proofs.

CRediT authorship contribution statement

Ningning Li: Methodology, Formal analysis, Investigation. **Huibo Jin:** Methodology, Formal analysis, Investigation. **Hongbo Li:** Investigation. **Huilin Yu:** Investigation. **Xiaoxu Wu:** Investigation. **Tianci Zhang:** Investigation. **Liangliang Yu:** Supervision. **Zhaoling Qin:** Methodology. **Li Luo:** Conceptualization, Data curation, Formal analysis, Funding acquisition, Investigation, Methodology, Supervision, Writing – review & editing.

Declaration of competing interest

The authors declare that they have no competing interests that could have appeared to influence the work reported in this paper.

Acknowledgements

This research was supported by the Natural Science Foundation of China (31570241 to L. L.).

Supplementary materials

Supplementary material associated with this article can be found, in the online version, at doi:10.1016/j.crmicr.2025.100345.

Data availability

Data will be made available on request.

References

Balandina, A., Claret, L., Hengge-Aronis, R., Rouviere-Yaniv, J., 2001. The Escherichia coli histone-like protein HU regulates rpoS translation. Mol. Microbiol. 39, 1069–1079.
Balandina, A., Kamashev, D., Rouviere-Yaniv, J., 2002. The bacterial histone-like protein HU specifically recognizes similar structures in all nucleic acids - DNA, RNA, and their hybrids. J. Biol. Chem. 277, 27622–27628.
Calatrava-Morales, N., Nogales, J., Ameztoy, K., van Steenbergen, B., Soto, M.J., 2017. The NtrY/NtrX system of sinorhizobium meliloti GR4 regulates motility, EPS I production, and nitrogen metabolism but is dispensable for symbiotic nitrogen fixation. Mol. Plant-Microbe Interactions 30, 566–577.
Carabetta, V.J., 2021. Addressing the possibility of a histone-like code in bacteria. J. Proteome Res. 20, 27–37.
Felletti, M., Omnus, D.J., Jonas, K, 2019. Regulation of the replication initiator DnaA in Caulobacter crescentus. Biochimica Et Biophysica Acta-Gene Regulatory Mechanisms 1862, 697–705.
Fernandez, I., Cornaciu, I., del, Carmen, Carrica, M., Uchikawa, E., Hoffmann, G., Sieira, R., Marquez, J.A., Goldbaum, F.A., 2017. Three-dimensional structure of full-length NtrX, an unusual member of the NtrC Family of response regulators. J. Mol. Biol. 429, 1192–1212.
Fioravanti, A., Fumeaux, C., Mohapatra, S.S., Bompard, C., Brilli, M., Frandi, A., Castric, V., Villeret, V., Viollier, P.H., Biondi, E.G., 2013. DNA binding of the cell cycle transcriptional regulator GcrA depends on N6-adenosine methylation in Caulobacter crescentus and other Alphaproteobacteria. PLoS Genet. 9.
Hammel, M., Amlanjyoti, D., Reyes, F.E., Chen, J.-H., Parpana, R., Tang, H.Y.H., Larabell, C.A., Tainer, J.A., Adhya, S., 2016. HU multimerization shift controls nucleoid compaction. Sci. Adv. 2.
Holowka, J., Trojanowski, D., Ginda, K., Wojtas, B., Gielniewski, B., Jakimowicz, D., Zakrzewska-Czerwinska, J., 2017. HupB is a bacterial nucleoid-associated protein with an indispensable eukaryotic-like tail. Mbio 8.
Kamashev, D., Rouviere-Yaniv, J., 2000. The histone-like protein HU binds specifically to DNA recombination and repair intermediates. Embo J. 19, 6527–6535.
Kano, Y., Yoshino, S., Wada, M., Yokoyama, K., Nobuhara, M., Imamoto, F., 1985. Molecular cloning and nucleotide sequence of the HU-1 gene of Escherichia coli. Mol. Gen. Genet. 201, 360–362.
Karaboja, X., Wang, X., 2022. HBsu is required for the initiation of DNA replication in Bacillus subtilis. J. Bacteriol. 204.
Kim, D-H, Im, H., Jee, J.-G., Jang, S.-B., Yoon, H.-J., Kwon, A.-R., Kang, S.-M., Lee, B.-J., 2014. β-arm flexibility of HU from Staphylococcus aureus dictates the DNA-binding and recognition mechanism. Acta Crystallographica Section D-Struct. Biol. 70, 3273–3289.

Kohler, P., Marahiel, M.A., 1997. Association of the histone-like protein HBsu with the nucleoid of Bacillus subtilis. J. Bacteriol. 179, 2060–2064.
Köhler, P., Marahiel, M.A., 1998. Mutational analysis of the nucleoid-associated protein HBsu of Bacillus subtilis. Mol. Gen. Genet. 260, 487–491.
Leigh, J.A., Signer, E.R., Walker, G.C., 1985. Exopolysaccharide-deficient mutants of Rhizobium meliloti that form ineffective nodules. Proc. Natl. Acad. Sci. U S A 82, 6231–6235.
Liao, J.-H., Tsai, C.-H., Patel, S.G., Yang, J.-T., Tu, I.F., Lo Cicero, M., Lipka-Lloyd, M., Wu, W.-L., Shen, W.-J., Ho, M.-R., Chou, C.-C., Sharma, G.R., Okanishi, H., Luk, L.Y. P., Tsai, Y.-H., Wu, S.-H, 2017. Acetylome of Acinetobacter baumannii SK17 reveals a highly-conserved modification of histone-like protein HU. Front. Mol. Biosci. 4.
Martinez-Val, A., Garcia, F., Ximenez-Embun, P., Martinez Teresa-Calleja, A., Ibarz, N., Ruppen, I., Munoz, J, 2017. Urea artifacts interfere with immuno-purification of lysine acetylation. J. Proteome Res. 16, 1061–1068.
McAdams, H.H., Shapiro, L., 2009. System-level design of bacterial cell cycle control. FEBS Lett. 583, 3984–3991.
Micka, B., Marahiel, M.A., 1992. The DNA-binding protein HBsu is essential for normal growth and development in Bacillus subtilis. Biochimie 74, 641–650.
Pini, F., De Nisco, N.J., Ferri, L., Penterman, J., Fioravanti, A., Brilli, M., Mengoni, A., Bazzicalupo, M., Viollier, P.H., Walker, G.C., Biondi, E.G., 2015. Cell cycle control by the master regulator CtrA in Sinorhizobium meliloti. Plos Genet. 11.
Prieto, A.I., Kahramanoglou, C., Ali, R.M., Fraser, G.M., Seshasayee, A.S.N., Luscombe, N.M., 2012. Genomic analysis of DNA binding and gene regulation by homologous nucleoid-associated proteins IHF and HU in Escherichia coli K12. Nucleic Acids Res. 40, 3524–3537.
Remesh, S.G., Verma, S.C., Chen, J.-H., Ekman, A.A., Larabell, C.A., Adhya, S., Hammel, M., 2020. Nucleoid remodeling during environmental adaptation is regulated by HU-dependent DNA bundling. Nat. Commun. 11.
Schafer, A., Tauch, A., Jager, W., Kalinowski, J., Thierbach, G., Puhler, A., 1994. Small mobilizable multi-purpose cloning vectors derived from the Escherichia coli plasmids pK18 and pK19: selection of defined deletions in the chromosome of Corynebacterium glutamicum. Gene 145, 69–73.
Schallies, K.B., Sadowski, C., Meng, J., Chien, P., Gibson, K.E., 2015. Sinorhizobium meliloti CtrA stability is regulated in a CbrA-dependent manner that is influenced by CpdR1. J. Bacteriol. 197, 2139–2149.
Stojkova, P., Spidlova, P., Stulik, J., 2019. Nucleoid-associated protein HU: a lilliputian in gene regulation of bacterial virulence. Front. Cell Infect. Microbiol. 9.
Swinger, K.K., Rice, P.A., 2004. IHF and HU: flexible architects of bent DNA. Curr. Opin. Struct. Biol. 14, 28–35.
Tang, G., Xing, S., Wang, S., Yu, L., Li, X., Staehelin, C., Yang, M., Luo, L., 2017. Regulation of cysteine residues in LsrB proteins from sinorhizobium meliloti under free-living and symbiotic oxidative stress. Environ. Microbiol. 19, 5130–5145.
van Teeseling, M.C.F., Thanbichler, M., 2020. Generating asymmetry in a changing environment: cell cycle regulation in dimorphic alphaproteobacteria. Biol. Chem. 401, 1349–1363.
Wang, D., Xue, H., Wang, Y., Yin, R., Xie, F., Luo, L., 2013. The Sinorhizobium meliloti ntrX gene is involved in succinoglycan production, motility, and symbiotic nodulation on alfalfa. Appl. Environ. Microbiol. 79, 7150–7159.
Xing, S., Zheng, W., An, F., Huang, L., Yang, X., Zeng, S., Li, N., Ouenzar, K., Yu, L., Luo, L., 2022. Transcription regulation of cell cycle regulatory genes mediated by ntrx to affect sinorhizobium meliloti cell division. Genes 13.
Xue, S., Biondi, E.G., 2019. Coordination of symbiosis and cell cycle functions in Sinorhizobium meliloti. Biochimica Et Biophysica Acta-Gene Regulatory Mech. 1862, 691–696.